Exact Traversable Wormhole Solutions in Finsler-Randers Gravity: Geometry, Physical Viability, and Equilibrium

Shahid Hussain Gurmani[1†] Allah Ditta[2,3‡] Imtiaz Khan[4§] Alisher Abduvokhidov[5,6♮] Chengxun Yuan[7♯] Ahmadjon Abdujabbarov[7,8,9¶]

[1]School of Computer Information Engineering, Shanxi Technology and Business University, Taiyuan, 030006, People's Republic of China
[2]Department of Mathematics, School of Science, University of Management and Technology, Lahore, 54000, Pakistan
[3]Research Center of Astrophysics and Cosmology, Khazar University, Baku, AZ1096, 41 Mehseti Street, Azerbaijan
[4]Department of Physics, Zhejiang Normal University, Jinhua, Zhejiang 321004, China
[5]Andijan State University, Universitet Str. 129, Andijan 170100, Uzbekistan
[6]University of Tashkent for Applied Sciences, Str. Gavhar 1, Tashkent 100149, Uzbekistan
[7]School of Physics, Harbin Institute of Technology, Harbin 150001, People's Republic of China
[8]Institute of Fundamental and Applied Research, National Research University TIIAME, Kori Niyoziy 39, Tashkent 100000, Uzbekistan
[9]National University of Uzbekistan, Tashkent 100174, Uzbekistan

CPC Accepted

Abstract: We construct a static, spherically symmetric traversable wormhole in Finsler–Randers (FR) gravity using the osculating-Riemannian formulation, in which spacetime anisotropy is encoded by a weak timelike vector field $\zeta_a(r)$ rather than introduced phenomenologically at the matter level. Starting from the general FR field equations for a static, spherically symmetric line element, we specialize to a zero-tidal-force Morris–Thorne wormhole and derive closed-form expressions for the energy density, radial pressure, and tangential pressure sourcing a fixed shape function $b(r) = r_0^2/r$. Adopting a decaying weak-field ansatz for the anisotropy field, $\zeta_0(r) = \zeta_c r_0/r$, we show that the amount of null-energy-condition (NEC)-violating matter required to keep the throat open decreases monotonically with ζ_c. We also show that the radial extent of the NEC-violating region shrinks from the entire spacetime in the general-relativistic limit $\zeta_c \to 0$ to a compact neighborhood of the throat, within the weak-anisotropy range identified below as the regime in which our quantitative results are reliable. We further derive the generalized hydrostatic-equilibrium (TOV-type) equation for this geometry and identify an explicit geometric force F_ζ, sourced by the gradient of $\zeta_0(r)$, that supplements the usual hydrostatic and anisotropic forces. The model reduces smoothly to the general-relativistic Morris–Thorne wormhole as $\zeta_0 \to 0$, and all reported effects remain within the weak-anisotropy regime $|\zeta_0| \ll 1$ under which the field equations were derived. We also examine tidal forces, finding that the radial component vanishes identically for all observers. In addition, we analyze sound speeds and the Herrera cracking criterion, restricted to its domain of validity; a corrected, convergent exotic-matter measure evaluated over the NEC-violating shell itself, which we adopt as our primary quantifier of exotic-matter content; a Herrera-type complexity factor adapted to the wormhole geometry; an analytic classification of the critical anisotropy strength across the shape-function and anisotropy-decay parameter space; a thin-shell realization with reduced surface exotic density; the absence of a photon sphere and the corresponding light-deflection angle; a linearized generalization to a nonzero redshift function; and a comparison with wormhole constructions in other modified-gravity theories.

Keywords: Wormhole Solutions, Finsler–Randers Gravity, osculating-Riemannian formulation

DOI: 10.1088/1674-1137/aeb3ef **CSTR:**

I. INTRODUCTION

The idea that spacetime might admit a tunnel-like passage connecting two otherwise separate regions goes back to Flamm's 1916 embedding of the Schwarzschild solution and was given its first field-theoretic treatment by Einstein and Rosen, who joined two copies of the Schwarzschild exterior along their horizon to remove the

Received 27 July 2026; Accepted 13 October 2026

† E-mail: shahidgurmani07@gmail.com
‡ E-mail: mradshahid01@gmail.com
§ E-mail: ikhanphys1993@gmail.com (Corresponding Author)
♮ E-mail: alisher˙abdulvoxidov@adu.uz
♯ E-mail: yuancx@hit.edu.cn (Corresponding Author)
¶ E-mail: ahmadjonab@gmail.com

©2026 Chinese Physical Society and the Institute of High Energy Physics of the Chinese Academy of Sciences and the Institute of Modern Physics of the Chinese Academy of Sciences and IOP Publishing Ltd. All rights, including for text and data mining, AI training, and similar technologies, are reserved.

central singularity and represent a particle as a smooth "bridge" between sheets [15]. Wheeler later termed such handles in the topology of space "geons" and gave the first explicit picture of a tunnel connecting distant regions [16]. These constructions were not traversable: the Einstein–Rosen bridge pinches off before a signal can cross it. The modern notion of a *traversable* wormhole, held open long enough for a physical observer to pass through, was formulated by Morris and Thorne [1], who showed that a static, spherically symmetric throat connecting two asymptotically flat regions requires a flare-out condition on the shape function $b(r)$ that in general relativity (GR) forces violation of the null energy condition (NEC) at or near the throat [2]. Morris, Thorne, and Yurtsever additionally showed that a traversable wormhole could in principle be converted into a time machine, tying the subject to deep and still unresolved questions about causality and quantum field theory in curved spacetime [17]. Subsequent work developed the thin-shell formalism for confining the exotic content to a shell via Darmois–Israel matching [18], examined the physical consequences of converting a wormhole into a time machine [19], and established the generic geometric structure of static and dynamic wormhole throats and the energy conditions they must violate [20−22]. This body of work established two complementary responses to the exotic-matter requirement: sourcing wormholes with genuinely exotic but quantum-field-theoretically motivated stresses (Casimir energy, phantom fields), or reproducing the effective stress-energy needed for a wormhole throat purely geometrically, within modified or extended theories of gravity, so that the "exotic" content is an artefact of the extra geometric degrees of freedom rather than of new matter.

The second route has been pursued across essentially every major extension of GR. Reviews of $f(R)$ gravity [23], of the broader landscape of modified gravity and cosmology [25, 26], and of unified descriptions of the cosmic expansion history within curvature-based extensions [24] set out the general motivation: late-time cosmic acceleration, the dark-matter problem, and the search for a consistent ultraviolet completion of gravity all point toward extra geometric degrees of freedom beyond the Einstein–Hilbert action. Concretely, $f(R,T)$ gravity couples the Ricci scalar to the trace of the stress-energy tensor [27], building on earlier work allowing an arbitrary coupling between matter and geometry [28, 29]; symmetric teleparallel $f(Q)$ gravity recasts gravity in terms of the non-metricity scalar within a coincident, torsion-free and curvature-free connection [30], with a further matter-coupled extension to $f(Q,T)$ [31]; and teleparallel $f(T)$ gravity replaces curvature with torsion as the origin of gravitation [32, 33]. Wormhole solutions have been constructed in essentially all of these frameworks: in $f(R)$ gravity, where the higher-order curvature terms in the field equations can support a throat with matter that itself respects the null and weak energy conditions [34, 35]; in $f(R,T)$ gravity, where several independent constructions again find matter-satisfying solutions or wormholes with only localized, reduced energy-condition violation [36−39]; in Rastall gravity, where the non-conserved stress-energy tensor supplies an additional geometric source term [40, 41]; and, most recently, in symmetric teleparallel $f(Q)$ gravity [42]. Across this literature, the recurring finding is that a geometric modification of the field equations can substantially reduce, and in specific models eliminate, the amount of exotic matter a fixed wormhole geometry requires.

Finsler geometry generalizes Riemannian geometry by letting the metric depend on both position and direction on the tangent bundle [4, 43, 44]. The Finsler–Randers (FR) subclass, obtained by a linear deformation of a Riemannian metric with a one-form ζ_a [3], was developed into a cosmological framework through a sequence of work on Friedmann-like models with weak intrinsic anisotropy [45], imperfect fluids and Lorentz-violating extensions [47], and general very special relativity in a Finslerian setting [46]. Subsequent work addressed the weak-field limit and its Raychaudhuri equation [5], dark-energy-mimicking and DGP-equivalent Finsler–Randers cosmologies [6, 49], relativistic Finsler geometry more broadly [48], scalar-tensor extensions of the Raychaudhuri equation in FR spacetime [50], varying-vacuum FR cosmology [51], and, most recently, FR-Sasaki gravity and cosmology [52]. Beyond cosmology, the same osculating-Riemannian construction has produced Schwarzschild-like and black-hole solutions [53−56], anisotropic compact-star models in which the stellar anisotropy arises directly from the underlying Finslerian geometry rather than being imposed by hand [7, 8, 57], and, closest to the present work, Finslerian wormholes constructed by prescribing a Finslerian modification of an otherwise standard Morris–Thorne throat [9−11].

This body of work motivates the present study directly. Wormholes in modified gravity theories have repeatedly been shown to require less exotic matter, or none at all, than their GR counterparts [35, 42]; and Finsler–Randers anisotropy, in an entirely independent line of work, has been shown to increase the maximum supported mass and moment of inertia of compact stars relative to GR, again by supplying an additional geometric source term rather than additional matter [12]. The natural question – whether the same FR anisotropy field can similarly reduce the exotic-matter requirement of a fixed wormhole geometry – has, to our knowledge, not been addressed using the specific FR field equations of Ref. [12], which were derived for a completely general static, spherically symmetric metric under the weak-anisotropy, osculating-Riemannian approximation. In this work we specialize those field equations – for the first

CPC Accepted

time, to our knowledge, in closed analytic form – to a Morris–Thorne wormhole geometry. Because the field equations were derived independently of any stellar-specific ansatz, they apply unchanged to the wormhole metric once the metric potentials are replaced by the shape function $b(r)$ and redshift function $\Phi(r)$. This lets us isolate, in a controlled and reproducible way, exactly how the FR anisotropy field $\zeta_0(r)$ redistributes the stress-energy required to support a fixed wormhole geometry, and in particular how it affects the amount and radial extent of NEC violation.

The remainder of the paper is organized as follows. Section II summarizes the FR geometric framework and the general field equations. Section III specializes these to a zero-tidal-force wormhole and derives closed-form matter functions for a specific shape function and anisotropy ansatz. Section IV analyses the energy density, pressures, energy conditions, anisotropy, embedding diagram, and the amount of exotic matter as functions of the FR anisotropy parameter. Section V derives the generalized hydrostatic-equilibrium equation and the associated geometric force. Section VI extends the analysis to tidal forces, sound speeds, a corrected exotic-matter measure, a complexity factor, the shape-function and anisotropy-decay parameter space, a thin-shell realization, light deflection, and a comparison with other modified-gravity wormhole constructions. Section VII summarizes our results and discusses the regime of validity of the weak-anisotropy approximation.

II. FINSLER–RANDERS GEOMETRIC FRAMEWORK

We adopt the osculating-Riemannian formulation of FR gravity, in which the Finsler–Randers structure

$$L(u,v) = \sqrt{g_{ab}v^a v^b} + \zeta_a v^a \tag{1}$$

is evaluated along the fluid four-velocity v^a, yielding an effective Riemannian metric $f_{ab}(u)$ that reflects the underlying Finslerian anisotropy encoded in the one-form ζ_a. For a comoving observer, $v^a = (1,0,0,0)$. The weak, static anisotropy is characterized by a single radial function, $\zeta_a = (\zeta_0(r),0,0,0)$, with $|\zeta_0| \ll 1$ throughout.

For the static, spherically symmetric interior line element

$$ds^2 = e^{\mu(r)}dt^2 - e^{\eta(r)}dr^2 - r^2\left(d\theta^2 + \sin^2\theta\, d\varphi^2\right), \tag{2}$$

The field equations obtained from $R_{ab} = 8\pi G\left(T_{ab} - \frac{1}{2}T f_{ab}\right)$ under the weak-field osculating approximation ($C_{abc} \approx 0$) are given by [12]

$$8\pi\rho = \frac{1 - e^{-\eta} + e^{-\eta}r\eta'}{r^2} + \frac{e^{-\eta-\mu/2}\left(-2 + \frac{1}{2}r\eta' + r\mu'\right)\zeta_0'}{r}, \tag{3}$$

$$8\pi p_r = \frac{-2 + 2e^{-\eta} + 2e^{-\eta}r\mu'}{2r^2} + \frac{e^{-\eta-\mu/2}(3 + r\mu')\zeta_0'}{2r}, \tag{4}$$

$$8\pi p_t = \frac{1}{8r}\Big[e^{-\eta-\mu/2}(6 - 3r\eta' - 4r\mu')\zeta_0' + 2e^{-\eta}(\mu' - \eta')(2 + r\mu') + 2r\mu''\Big]. \tag{5}$$

These three relations hold for *any* choice of the metric potentials $\mu(r)$ and $\eta(r)$. In Ref. [12], they were combined with the Finch–Skea stellar ansatz. Here, we instead substitute the Morris–Thorne wormhole ansatz.

III. WORMHOLE CONSTRUCTION

The Morris–Thorne line element is

$$ds^2 = e^{2\Phi(r)}dt^2 - \frac{dr^2}{1 - b(r)/r} - r^2\left(d\theta^2 + \sin^2\theta\, d\varphi^2\right), \tag{6}$$

Thus, by comparison with Eq. (2),

$$\mu(r) = 2\Phi(r), \qquad e^{-\eta(r)} = 1 - \frac{b(r)}{r}. \tag{7}$$

We restrict attention to the zero-tidal-force case, $\Phi(r) \equiv 0$, which is standard in the wormhole literature and isolates the effect of the FR anisotropy field from that of a conventional gravitational redshift. Substituting $\mu = \mu' = \mu'' = 0$ into Eqs. (3)–(5) yields

$$8\pi\rho(r) = \frac{b'(r)}{r^2} + \frac{\zeta_0'(r)}{2r^2}\left[r\,b'(r) - 4r + 3b(r)\right], \tag{8}$$

$$8\pi p_r(r) = -\frac{b(r)}{r^3} + \frac{3\zeta_0'(r)}{2r^2}\left[r - b(r)\right], \tag{9}$$

$$8\pi p_t(r) = \frac{b(r) - r\,b'(r)}{2r^3} - \frac{3\zeta_0'(r)}{8r^2}\left[r\,b'(r) - 2r + b(r)\right]. \tag{10}$$

In the limit $\zeta_0 \to 0$, these equations reduce exactly to the standard general-relativistic Morris–Thorne relations, $8\pi\rho = b'/r^2$, $8\pi p_r = -b/r^3$, $8\pi p_t = (b - rb')/2r^3$, confirming the consistency of Eqs. (8)–(10) with GR in the appropriate limit.

A. Shape function and anisotropy ansatz

We adopt the simplest shape function that is compatible with a throat at $r = r_0$, asymptotic flatness, and the

CPC Accepted

flare-out condition.

$$b(r) = \frac{r_0^2}{r}, \tag{11}$$

for which $b(r_0) = r_0$ and $b'(r_0) = -1 < 1$. Thus, the flare-out condition is trivially satisfied, independently of the FR sector. The wormhole shape itself is fixed; instead, the matter content required to support this fixed shape is modified by the FR geometry.

For the anisotropy field, we adopt the simplest decaying, weak-field ansatz that is consistent with both the requirement $\zeta_0 \to 0$ far from the throat (thereby recovering GR asymptotically) and the regularity of the metric,

$$\zeta_0(r) = \zeta_c \frac{r_0}{r}, \tag{12}$$

where the dimensionless parameter $\zeta_c = \zeta_0(r_0)$ controls the strength of the Finslerian anisotropy at the throat. Consistency with the weak-field approximation underlying Eqs. (3)–(5) requires $\zeta_c \ll 1$. We therefore quantify the results for $\zeta_c \in \{0, 0.15, 0.3, 0.45, 0.6\}$ and discuss the formal limit $\zeta_c \to 2$ in Sec. VII only as a mathematical boundary of the model, not as a physically admissible regime.

Because the field equations in Eqs. (3)–(5) retain only the leading terms in ζ_0 and its derivative, the fractional size of the FR correction to any GR matter function is, by construction, of order ζ_c at the throat. Moreover, Eqs. (13)–(15) below are manifestly linear in ζ_c at fixed r/r_0. We regard $\zeta_c \lesssim 0.3$ as the practical range in which the quantitative trends reported below can be trusted within the weak-field approximation used to derive Eqs. (3)–(5). In this range, the linear corrections to ρ, p_r, and p_t at the throat remain below roughly 30% of the leading GR terms. The larger values $\zeta_c = 0.45$ and $\zeta_c = 0.6$ are retained in the figures because they make the systematic trend with ζ_c visually unambiguous across an extended set of diagnostics. Wherever a specific number is quoted for these larger values–for instance, $r_*(\zeta_c)$ in Table I–it should be interpreted as an extrapolation of the linear-order formulas rather than as a quantitative prediction of the full nonlinear theory, whose $O(\zeta_0^2)$ and Cartan-torsion corrections we have not computed. Strictly, only the formal limit $\zeta_c \to 0$ and its immediate neighborhood are guaranteed to satisfy $|\zeta_0| \ll 1$. The monotonic *trends* we report are, in our view, substantially more robust than any single quoted number at $\zeta_c \gtrsim 0.5$, and we consistently flag this distinction wherever such values are discussed below.

Substituting $b(r) = r_0^2/r$ and Eq. (12) into Eqs. (8)–(10) gives the closed-form matter functions

$$8\pi\rho(r) = \frac{r_0\left[\zeta_c(2r^2 - r_0^2) - r\,r_0\right]}{r^5}, \tag{13}$$

Table 1. Radius r_* (in units of r_0) at which $\rho + p_r$ changes sign for the shape function $b = r_0^2/r$ and the anisotropy ansatz $\zeta_0 = \zeta_c r_0/r$.

ζ_c	r_*/r_0
0.0	— (NEC violated for all r)
0.2	19.95
0.4	9.90
0.6	6.51
0.8	4.79
1.0	3.73
1.5	2.22
≥ 2.0	— (NEC satisfied for all r)

$$8\pi p_r(r) = -\frac{r_0\left[2r\,r_0 + 3\zeta_c(r^2 - r_0^2)\right]}{2r^5}, \tag{14}$$

$$8\pi p_t(r) = \frac{r_0(4r_0 - 3r\zeta_c)}{4r^4}. \tag{15}$$

B. Effective Finslerian shape function

The functions $b(r)$ and $\eta(r)$ appearing in Eqs. (8)–(10) parameterize the osculating Riemannian metric g_{ab} used to construct the field equations; they are independent of ζ_c. However, the physically measured Finsler–Randers metric is f_{ab}, not g_{ab}. Specializing Eqs. (14)–(15) of Ref. [12] to $\mu = 0$ gives

$$f_{rr} = e^{\eta(r)}\left(1 + \zeta_0(r)\right), \tag{16}$$

Thus, the radial sector of the *physical* wormhole geometry is distorted by the anisotropy field, although $b(r)$ itself remains unchanged. We define an effective, ζ_c-dependent shape function by writing $f_{rr} \equiv \left[1 - b_{\rm eff}(r)/r\right]^{-1}$, which captures this distortion. For $b(r) = r_0^2/r$ and $\zeta_0(r) = \zeta_c r_0/r$, this yields the following closed-form expression

$$b_{\rm eff}(r) = \frac{r_0(\zeta_c\, r + r_0)}{r + \zeta_c\, r_0}. \tag{17}$$

It is straightforward to verify that $b_{\rm eff}(r_0) = r_0$ for every ζ_c; thus, the throat location is unaffected by the FR field. Moreover, $b_{\rm eff} \to r_0^2/r$ as $\zeta_c \to 0$, recovering $b(r)$, and the flare-out condition generalizes to $b'_{\rm eff}(r_0) = (\zeta_c - 1)/(\zeta_c + 1) < 1$ for all $\zeta_c \geq 0$. Hence, the flare-out condition holds throughout the family. We use $b_{\rm eff}(r)$, rather than the bare $b(r)$, in Figs. 1 and 2 below because $b_{\rm eff}$ governs the actual embedded geometry of the throat. The function $b(r)$ itself is retained as the source of the matter functions in Eqs. (13)–(15), consistent with its role in the field

CPC Accepted

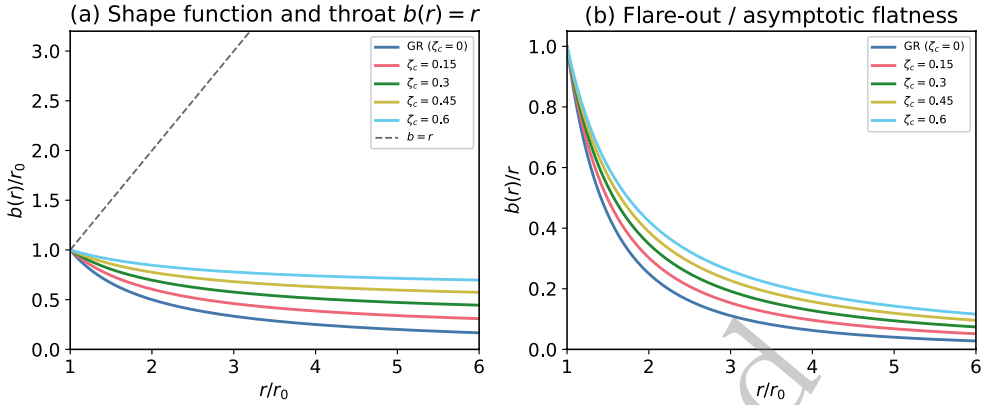


Fig. 1. (color online) (a) Effective shape function $b_{\rm eff}(r)$, Eq. (17), and the line $b = r$; their intersection marks the throat at $r = r_0$ for each ζ_c. (b) Ratio $b_{\rm eff}(r)/r$, confirming asymptotic flatness.

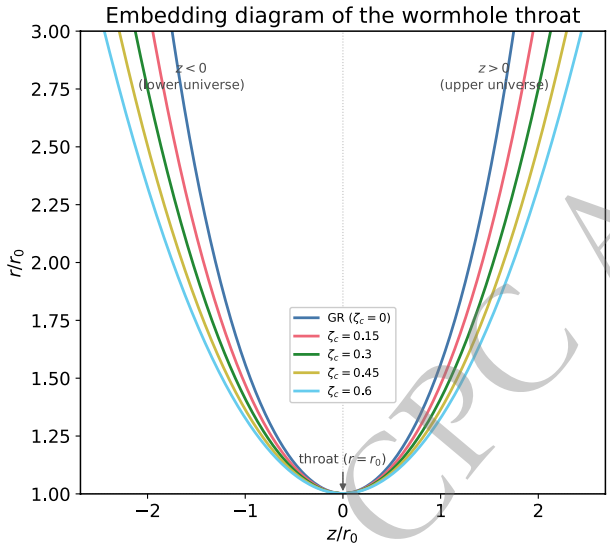


Fig. 2. (color online) Embedding diagram of the wormhole throat using the effective shape function $b_{\rm eff}(r)$ in the GR limit and for four Finslerian values. The two branches, $z < 0$ and $z > 0$, represent the two asymptotically flat regions joined at the throat $r = r_0$, $z = 0$; by construction, they are mirror images of each other. Increasing ζ_c widens the embedded throat profile for fixed r while leaving the throat location r_0 unchanged.

equations. We emphasize that this is a radial-sector diagnostic: the angular sector of f_{ab} is also rescaled, $f_{\theta\theta} = r^2(1+\zeta_0)$, which would shift the areal radius itself under a full reparametrization. We leave such a fully self-consistent treatment for future work. Accordingly, every subsequent result that relies on $b_{\rm eff}(r)$, rather than on the bare matter functions in Eqs. (13)–(15), should be interpreted as a leading-order, radial-sector approximation to the physical FR geometry rather than as an exact statement. This applies specifically to the embedding diagrams in Fig. 2, the lateral tidal force in Eq. (20), the thin-shell surface density in Eq. (26), and the light-deflection angle in Eq. (27). A fully self-consistent construction that uses f_{rr} and $f_{\theta\theta}$ together to redefine the areal radius and the observers' proper distances could shift each of these quantities by terms of order ζ_0. We expect the qualitative trends reported for these quantities–the widening of the embedded throat, the growth of the lateral tidal force and the deflection angle with ζ_c, and the reduction of the thin-shell density–to be robust, because they track the sign and monotonicity of $\zeta_0(r)$ itself rather than the specific radial-only construction of $b_{\rm eff}$. However, we do not claim that the curves shown in Figs. 2, 8, and 13 are exact.

IV. PHYSICAL ANALYSIS

A. Density, pressures, and anisotropy

Figure 1 shows the effective shape function $b_{\rm eff}(r)$, Eq. (17), together with the line $b = r$, whose intersection marks the throat, and the ratio $b_{\rm eff}(r)/r$, which confirms asymptotic flatness. Figure 2 shows the corresponding embedding diagrams. Both figures show the GR limit and four representative Finslerian cases, $\zeta_c \in \{0, 0.15, 0.3, 0.45, 0.6\}$. Increasing ζ_c visibly widens the embedded throat profile at fixed r, while leaving the throat location, r_0, unchanged. All r-dependent matter quantities below follow the same convention: the GR limit plus four Finslerian values. These cases remain within the weak-field range $\zeta_c \ll 1$ under which Eqs. (3)–(5) were derived. The radial window is restricted to the region where essentially all of the FR-versus-GR contrast occurs.

Figure 3 shows $\rho(r)$ from Eq. (13). The energy density remains negative near the throat for all values of ζ_c shown, but its magnitude is reduced relative to the GR curve. The FR correction also shifts the zero crossing of ρ inward as ζ_c increases.

Figure 4 shows the radial and tangential pressures separately. The magnitude of $p_r(r)$ is reduced by the FR correction over most of the range shown, whereas $p_t(r)$ is

CPC Accepted

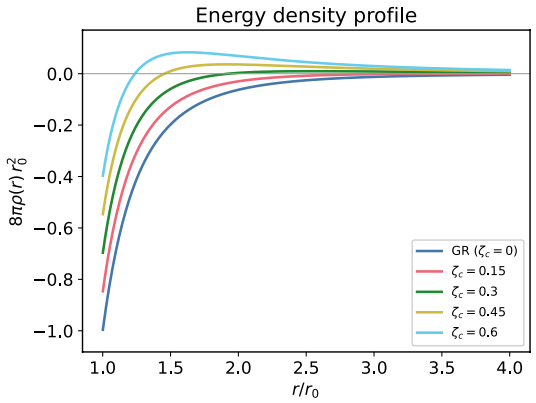


Fig. 3. (color online) Energy-density profile, Eq. (13), in the GR limit ($\zeta_c = 0$) and for four Finslerian values.

only mildly affected near the throat and becomes increasingly suppressed at larger r as ζ_c increases, consistent with the anisotropy analysis below.

B. Energy conditions and the amount of exotic matter

Figure 5(a) shows the radial NEC combination $\rho + p_r$. In the GR limit, $\rho + p_r = -2r_0^2/r^4 < 0$ everywhere, which is the standard Morris–Thorne result. As ζ_c increases, the NEC-violating region contracts from the entire radial range to a finite neighbourhood $r_0 \le r \le r_*(\zeta_c)$ around the throat, beyond which $\rho + p_r > 0$. Setting $\rho + p_r = 0$ in Eqs. (13)–(14) yields the quadratic condition

$$\zeta_c \left(r^2 + r_0^2\right) - 4 r r_0 = 0, \tag{18}$$

with roots $r_*/r_0 = \left[2 \pm \sqrt{4 - \zeta_c^2}\right]/\zeta_c$ when $\zeta_c \le 2$. For $\zeta_c > 2$, the discriminant is negative and $\rho + p_r > 0$ for all $r \ge r_0$; thus, the NEC is formally satisfied everywhere. Table I lists $r_*(\zeta_c)$ for representative values, and Fig. 6(b) shows the same quantity over a continuous range. Figure 5(b) shows the tangential combination $\rho + p_t$, which remains closer to the marginal value (≈ 0) throughout and is less sensitive to ζ_c than the radial sector.

To quantify the total amount of NEC-violating matter, we use the Visser-type volume integral [2]

$$I_V = \int_{r_0}^{r_0+\Delta} (\rho + p_r)\, r^2\, dr, \tag{19}$$

evaluated over a fixed reference shell $\Delta = 5r_0$. Figure 6(a) shows I_V as a function of ζ_c. The magnitude $|I_V|$ decreases monotonically as the FR anisotropy strengthens, quantifying the reduced amount of exotic matter required to keep the throat open. However, this fixed-shell measure is not physically well motivated: since $(\rho + p_r)r^2 \sim r_0\zeta_c/(2r)$ at large r (from Eqs. (13)–(14)), the integral I_V *diverges logarithmically* as $\Delta \to \infty$ for any $\zeta_c > 0$. Thus, extending it to an arbitrarily large shell is not meaningful. The appropriate convergent and physically motivated measure integrates only over the NEC-*violating* region, $[r_0, r_*(\zeta_c)]$, which is finite by construction; we return to this corrected measure in Sec. VI. We use that convergent measure, $I_V^{\rm shell}(\zeta_c)$, as our primary quantifier of exotic-matter content throughout the remainder of the paper. The fixed-shell value I_V discussed here is retained only for continuity with the reference-shell convention of Ref. [2] and is not used to support any quantitative claim below.

C. Anisotropy

The pressure anisotropy $\Delta(r) = p_t(r) - p_r(r)$, shown in Fig. 7, is generated solely by the FR geometric field. For $\zeta_c = 0$, Δ reduces to the nonzero GR Morris–Thorne anisotropy, whereas increasing ζ_c modifies both its sign structure and its magnitude near the throat. This behavior is consistent with the interpretation of $\zeta_0(r)$ as a direction-dependent geometric stress rather than a phenomenological matter anisotropy.

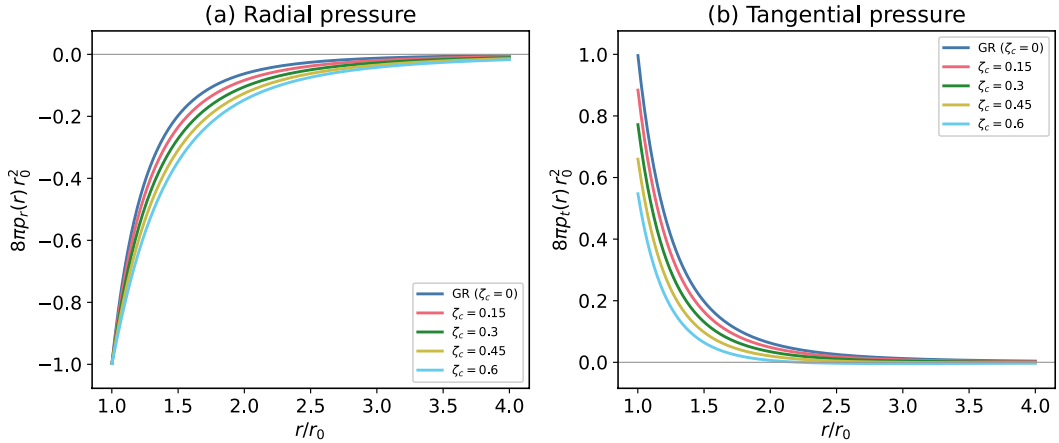


Fig. 4. (color online) (a) Radial pressure $p_r(r)$, given by Eq. (14). (b) Tangential pressure $p_t(r)$, given by Eq. (15). Both panels show the GR limit and the same four Finslerian values as in Fig. 3.

CPC Accepted

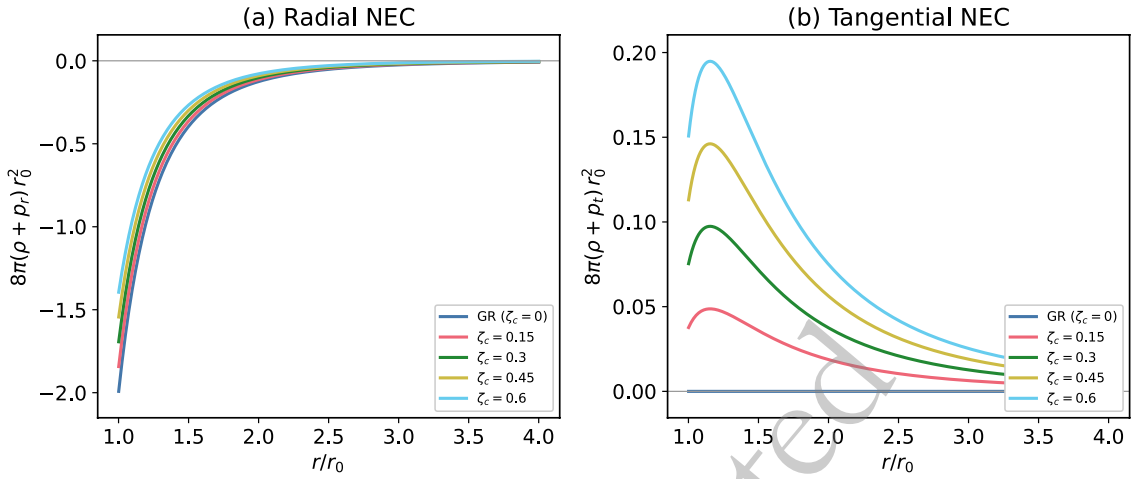


Fig. 5. (color online) (a) Radial NEC combination $\rho+p_r$: the GR curve is negative for all $r>r_0$, whereas increasing ζ_c progressively restores $\rho+p_r>0$ beyond a finite radius $r_*(\zeta_c)$. (b) Tangential NEC combination $\rho+p_t$.

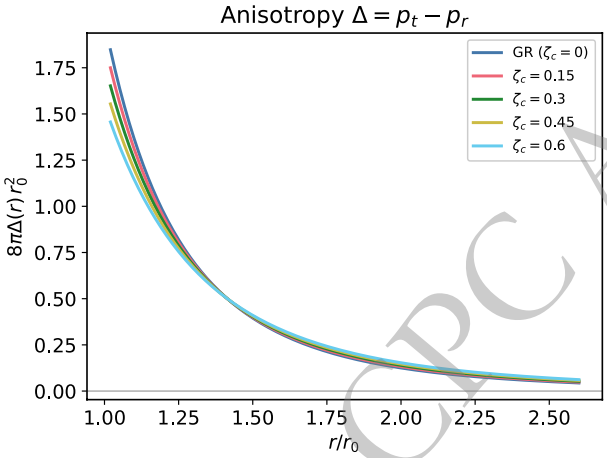


Fig. 6. (color online) (a) Exotic-matter quantifier $I_V(\zeta_c)$ over the fixed reference shell $\Delta=5r_0$: its magnitude decreases monotonically with increasing FR anisotropy strength (see the caution above regarding $\Delta\to\infty$). (b) Radial extent $r_*(\zeta_c)$ of the NEC-violating region, which vanishes (in the sense that $r_*\to r_0$) as $\zeta_c\to 2$.

D. Tidal forces

A wormhole is *traversable* in the sense originally intended by Morris and Thorne only if the tidal accelerations experienced by a traveler crossing the throat remain below human tolerance. We computed the relevant curvature components directly from the Riemann tensor of the metric in Eq. (2), rather than assuming a standard-form result, for both a static observer and an observer moving radially at velocity v with Lorentz factor γ. Two results follow. First, the *radial* tidal force depends only on Φ' and Φ'' and vanishes *identically* for the zero-tidal-force ansatz $\Phi\equiv 0$—for every ζ_c, every r, and every traveler velocity v, not merely for $v=0$. This is, after all, the defining property of a ``zero-tidal-force'' wormhole. Second, the lateral (tangential) tidal force does not vanish and is boost dependent,

$$\mathcal{F}_{\rm lat}(r,v)=\gamma^2v^2\,\frac{b_{\rm eff}(r)-r\,b'_{\rm eff}(r)}{2r^3}, \tag{20}$$

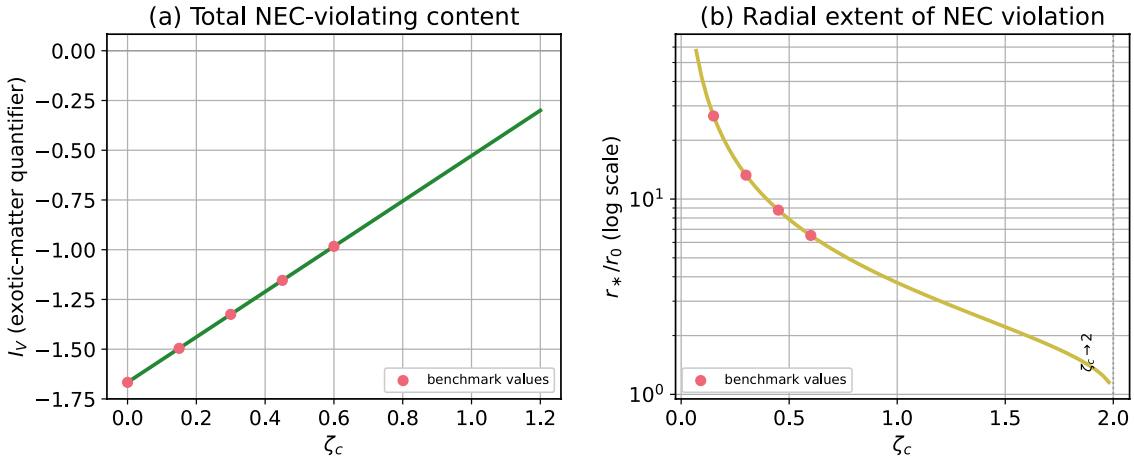


Fig. 7. (color online) Pressure anisotropy $\Delta=p_t-p_r$ for the same set of ζ_c values as in Fig. 3.

CPC Accepted

where we use the effective shape function $b_{\rm eff}(r)$ from Eq. (17), because tidal forces are measured by physical observers moving through the actual Finsler–Randers geometry. Figure 8 shows $\mathcal{F}_{\rm lat}$ for two representative crossing speeds. Increasing ζ_c increases the magnitude of the lateral tidal force for fixed r and v. Thus, the trade-off for the reduced exotic-matter content identified in Sec. IV is a somewhat less gentle passage for a traveler moving rapidly through the throat, although the effect remains small for the weak-field ζ_c values considered here.

E. Equation of state and sound speed

The equation-of-state parameters $\omega_r = p_r/\rho$ and $\omega_t = p_t/\rho$, the radial and tangential sound speeds $v_r^2 = dp_r/d\rho$ and $v_t^2 = dp_t/d\rho$, and the associated Herrera cracking combination $v_t^2 - v_r^2$ [13] are standard diagnostics for anisotropic relativistic matter. For our closed-form expressions for ρ, p_r, p_t, these quantities can all be computed straightforwardly. However, an important subtlety arises: both diagnostics require division by ρ or by $d\rho/dr$, and $\rho(r)$ is *non-monotonic* for any $\zeta_c > 0$ (Fig. 3 already shows that it crosses zero and has a turning point). Consequently, $\omega_{r,t}$ diverge at the radius $r_{\rho=0}(\zeta_c)$ at which ρ vanishes, and $v_{r,t}^2$ diverge at the generally smaller radius $r_{\rm infl}(\zeta_c)$ at which $d\rho/dr = 0$. Beyond these radii, the diagnostics are not merely large but formally ill-defined, since $dp/d\rho$ presupposes an invertible $\rho(r)$. We therefore show each curve in Fig. 9 only up to its corresponding validity radius, rather than allowing it to approach a spurious divergence. In the GR limit, before any FR correction is applied, the standard $b = r_0^2/r$ Morris–Thorne choice already yields $\omega_r = 1$ and $\omega_t = -1$ identically for all r (a stiff radial fluid and a cosmological-constant-like tangential component), and correspondingly $v_r^2 = 1$ and $v_t^2 = -1$ exactly. This is a known limitation of this widely used textbook shape function, reflecting that ρ, p_r, p_t are reverse-engineered from a metric ansatz rather than derived from a single covariant equation of state. Turning on ζ_c does not remove this limitation; instead, it reduces the domain over which the sound-speed diagnostic is meaningful, since $r_{\rm infl}(\zeta_c)$ decreases with ζ_c (from $\approx 4.6\,r_0$ at $\zeta_c = 0.15$ to $\approx 1.6\,r_0$ at $\zeta_c = 0.6$). We report this transparently rather than omit it: it is a genuine limitation of this benchmark shape function, not of the FR framework itself, and the same caution applies equally to the GR solution to which it reduces. Because both diagnostics are restricted to $r \le \min(r_{\rho=0}, r_{\rm infl})$, the Herrera cracking combination $v_t^2 - v_r^2$ shown in Fig. 9(d) can be interpreted only as a local stability indicator within that restricted domain. It does not, and cannot, constitute a statement about the stability of the complete wormhole configuration for all $r \ge r_0$: beyond $r_{\rm infl}(\zeta_c)$, the diagnostic itself is undefined rather than merely large, so no conclusion about cracking can be drawn there from the present analysis. A genuinely global stability statement would require a criterion that does not presuppose an invertible $\rho(r)$, which we leave for future work.

V. EQUILIBRIUM AND THE GEOMETRIC FORCE

In GR, hydrostatic equilibrium for an anisotropic fluid is expressed by the TOV balance $F_h + F_g + F_a = 0$, with $F_h = -dp_r/dr$, $F_g = -\frac{1}{2}\Phi'(\rho + p_r)$, and $F_a = (2/r)(p_t - p_r)$. Because Eqs. (8)–(10) are heuristic field equations constructed from the osculating Ricci tensor rather than derived from a diffeomorphism-invariant action, we do not assume *a priori* that this identity continues to hold when $\zeta_0(r) \neq 0$. Instead, we compute $F_h + F_g + F_a$ directly from Eqs. (13)–(15) (with $F_g = 0$ because $\Phi \equiv 0$) and find

$$F_h + F_a = \frac{3r_0\zeta_c\left(3r_0^2 - 2r^2\right)}{2r^6} \equiv -F_\zeta(r), \tag{21}$$

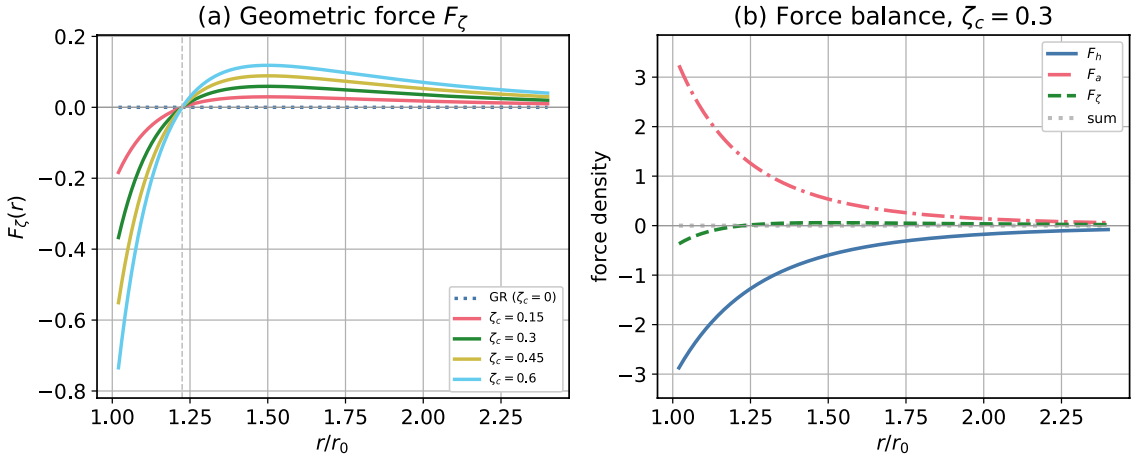


Fig. 8. (color online) Lateral tidal force $\mathcal{F}_{\rm lat}(r)$, Eq. (20), experienced by a traveler crossing with (a) $v = 0.5c$ and (b) $v = 0.99c$. The radial tidal force vanishes identically throughout (see text) and is therefore not plotted.

CPC Accepted

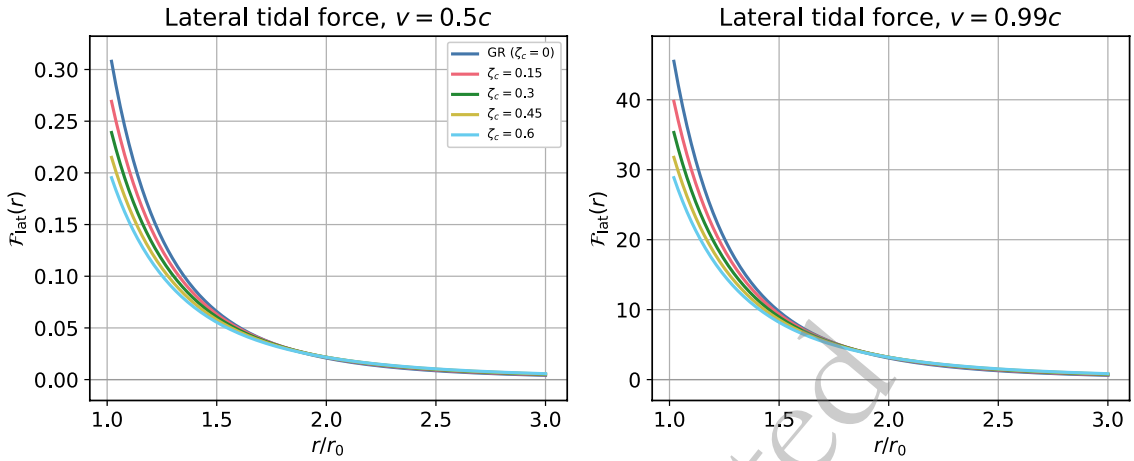


Fig. 9. (color online) (a)–(b) Radial and tangential equation-of-state parameters; each curve is truncated at its corresponding $\rho = 0$ radius. (c) Sound speeds v_r^2 (solid) and v_t^2 (dashed); each curve is truncated at its corresponding $d\rho/dr = 0$ radius, and dotted lines indicate the causal bounds 0 and 1. (d) Herrera cracking combination $v_t^2 - v_r^2$, with dotted lines at ± 1.

such that the generalized equilibrium condition becomes

$$F_h + F_g + F_a + F_\zeta = 0, \quad F_\zeta(r) = \frac{3r_0\zeta_c\left(2r^2 - 3r_0^2\right)}{2r^6}. \tag{22}$$

F_ζ vanishes identically when $\zeta_c = 0$; thus, it is a genuine geometric force sourced by the gradient of the Finslerian anisotropy field and is distinct from the pressure-anisotropy force F_a. Figure 10 shows the three forces and their sum, numerically confirming Eq. (22). We stress that F_ζ should not be interpreted as an independent material force arising from an additional matter component with its own equation of state. Once $b(r)$ and $\zeta_0(r)$ are fixed, Eqs. (8)–(10) completely determine ρ, p_r, and p_t. Therefore, F_ζ carries no independent degrees of freedom; it is simply the residual term obtained when the ordinary GR force balance $F_h + F_g + F_a$ is evaluated for this matter content and found not to vanish by itself. Instead, we interpret F_ζ as an effective geometric exchange term: a bookkeeping device for the momentum that the osculating-Riemannian construction transfers between the metric sector, encoded by $b(r)$, and the anisotropy sector, encoded by $\zeta_0(r)$, at fixed total matter content. This interpretation is analogous to the interaction term in a two-fluid or scalar-tensor system, which does not itself constitute a third independent source. It is also consistent with F_ζ vanishing identically whenever $\zeta_0 \equiv 0$ and with its sign reversal at $r = r_0\sqrt{3/2}$, which we take to indicate the radius where the direction of this geometric exchange reverses rather than where a new physical force switches on or off. In this sense, we interpret F_ζ as the direct mechanical action of the FR geometry on the fluid: for $\zeta_c > 0$, it changes sign at $r = r_0\sqrt{3/2}$, acts outward near the throat, and acts inward at larger radii. This behavior is consistent with the redistribution of the exotic-matter requirement described in Sec. IV.

VI. EXTENDED ANALYSIS

A. Corrected exotic-matter measure and complexity factor

As noted in Sec. IV, the fixed-shell quantifier I_V is not a physically principled measure of exotic-matter content because it diverges logarithmically as the shell size $\Delta \to \infty$. The appropriate convergent quantity integrates only over the NEC-violating region itself,

$$I_V^{\rm shell}(\zeta_c) = \int_{r_0}^{r_*(\zeta_c)} (\rho + p_r)\, r^2\, dr, \tag{23}$$

which is finite by construction because the domain of integration is bounded. Figure 11(a) shows $I_V^{\rm shell}(\zeta_c)$. This quantity retains the same qualitative and monotonic trend as in the fixed-shell version: the magnitude of the confined exotic-matter content decreases as ζ_c increases. However, it is now a well-defined, cutoff-independent result rather than an artifact of an arbitrarily chosen shell size.

We further evaluate the Herrera-type complexity factor [14], which, for a self-gravitating stellar configuration with a regular center, is usually written as $Y_{TF} = 8\pi\Pi - (4\pi/r^3)\int_0^r x^3\rho'(x)\,dx$, with $\Pi = p_t - p_r$. A wormhole has no regular center; its domain begins at the throat. We therefore adapt the definition by integrating the density gradient from r_0 rather than from 0,

$$Y_{TF}(r) = 8\pi\big(p_t(r) - p_r(r)\big) - \frac{4\pi}{r^3}\int_{r_0}^{r} x^3\rho'(x)\,dx, \tag{24}$$

This expression integrates to the closed form used in Fig. 11(b). Y_{TF} remains finite throughout and is systemat-

CPC Accepted

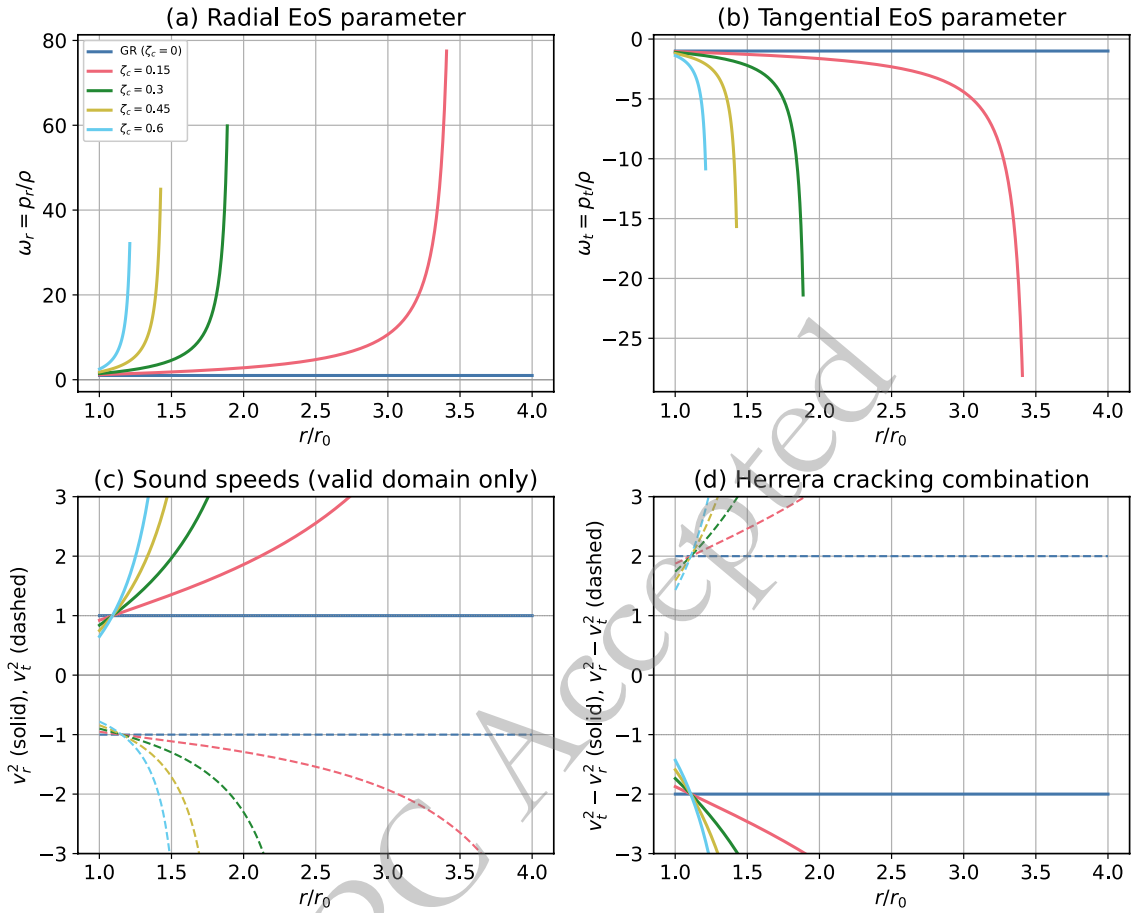


Fig. 10. (color online) (a) Geometric force $F_\zeta(r)$ in the GR limit and for four Finslerian values (it vanishes identically for $\zeta_c = 0$, as expected). (b) Force balance for the representative case $\zeta_c = 0.3$: hydrostatic (F_h), pressure-anisotropy (F_a), and geometric (F_ζ) contributions to Eq. (22). The dashed curve, representing their sum, vanishes identically, confirming equilibrium.

CPC Accepted

ically modified by ζ_c, providing a complementary single-function summary of how Finslerian anisotropy redistributes the configuration's structural complexity relative to GR.

B. Dependence on the shape-function and anisotropy-decay powers

The benchmark model uses $b(r) = r_0(r_0/r)^n$ and $\zeta_0(r) = \zeta_c(r_0/r)^k$ with $n = k = 1$. To assess how restrictive this choice is, we solved the generalized (n,k) field equations (a straightforward generalization of Eqs. (13)–(15)) and determined, for each (n,k), the value of ζ_c required to satisfy the radial NEC for *all* $r \geq r_0$. This is equivalent to finding the supremum over $r \geq r_0$ of

$$h(r;n,k) = \frac{2(n+1)\,r^k}{k(n+r^{n+1})}, \tag{25}$$

Since $\rho + p_r \geq 0$ for all r if and only if $\zeta_c \geq h(r;n,k)$ for all such r, three regimes emerge. We verified this classification against exhaustive numerical maximization over (n,k):

• For $k \leq 1$, the supremum is attained exactly at the throat, yielding the closed-form expression $\zeta_c^{\rm crit}(n,k) = 2/k$. This result is remarkably *independent of* n: the shape-function steepness does not affect the critical anisotropy strength, provided that the anisotropy field decays no faster than $1/r$. (This recovers $\zeta_c^{\rm crit} = 2$ for the benchmark case $n = k = 1$.)

• For $1 < k < n+1$, the supremum occurs at the interior radius $r_c = [kn/(n+1-k)]^{1/(n+1)} > r_0$. Thus, $\zeta_c^{\rm crit}(n,k) = h(r_c;n,k)$ is finite but requires a transcendental evaluation.

• For $k \geq n+1$, $h(r;n,k) \to \infty$ as $r \to \infty$: *no finite* ζ_c *can fully restore the NEC everywhere*. This occurs because a larger decay power k makes $\zeta_0(r) = \zeta_c(r_0/r)^k$ fall off *more rapidly*, not more slowly, as r increases. When $k \geq n+1$, the anisotropy field is driven toward zero faster than the shape function's own contribution to $\rho + p_r$ falls off. Consequently, at sufficiently large r, too little anisotropy remains to compensate for the residual NEC violation sourced by $b(r)$, regardless of how large ζ_c is made near the throat.

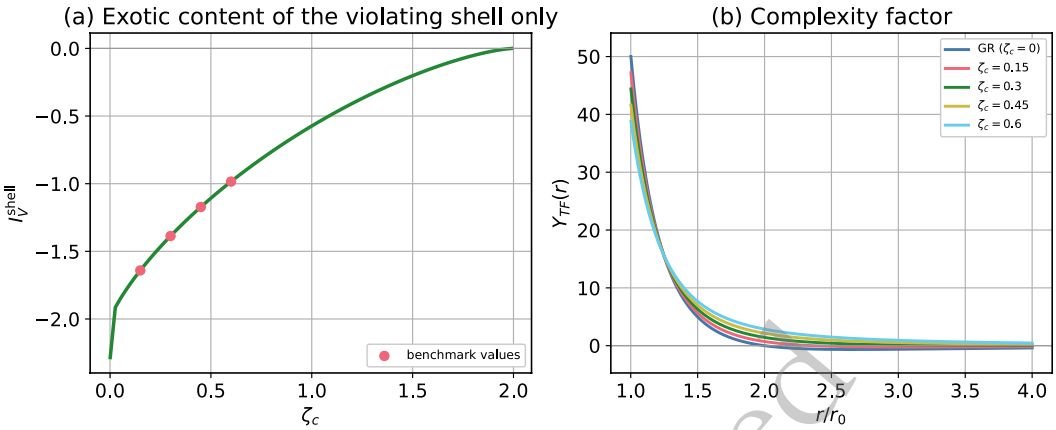


Fig. 11. (color online) (a) Corrected, convergent exotic-matter measure $I_V^{\rm shell}(\zeta_c)$, obtained by integrating only over the NEC-violating shell $[r_0, r_*(\zeta_c)]$. (b) Complexity factor $Y_{TF}(r)$, Eq. (24), adapted to a wormhole geometry.

Figure 12 shows $\zeta_c^{\rm crit}(n,k)$ in the (n,k) plane; the boundary $k = n+1$ marks the onset of the third regime.

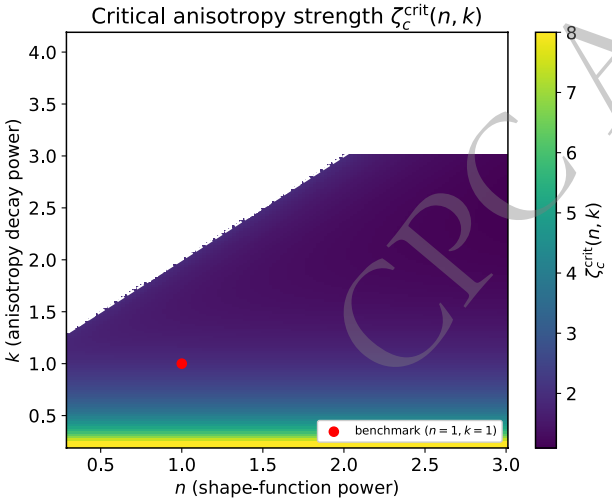


Fig. 12. (color online) Critical anisotropy strength $\zeta_c^{\rm crit}(n,k)$ required for the radial NEC to be satisfied for all $r \geq r_0$, as a function of the shape-function power n and the anisotropy-decay power k. Above the dashed line $k = n+1$, no finite ζ_c is sufficient. The red point indicates the benchmark model used throughout the remainder of this paper.

C. Thin-shell construction and optical properties

As an alternative to distributing the FR-modified matter throughout the bulk, one can confine it to a thin shell at a radius $R > r_0$ by gluing two identical copies of the exterior geometry at that surface (Darmois–Israel matching [2]). For our effective geometry, the resulting surface density is

$$\sigma(R) = -\frac{1}{2\pi R}\sqrt{1-\frac{b_{\rm eff}(R)}{R}} = -\frac{\sqrt{R^2-r_0^2}}{2\pi R^{3/2}\sqrt{R+\zeta_c r_0}}, \qquad (26)$$

which reduces to the standard Morris–Thorne thin-shell result when $\zeta_c = 0$. Because $b_{\rm eff}(R) \geq b(R)$ for $\zeta_c > 0$ (Sec. III B), the magnitude of the surface density, $|\sigma(R)|$, is *reduced* by the FR anisotropy at every shell radius. This mirrors the bulk result in Sec. IV: the exotic content needed to keep a wormhole open, whether distributed throughout the bulk or confined to a shell, decreases as ζ_c grows. Figure 13(a) shows $\sigma(R)$ in the GR limit and for four Finslerian values.

Regarding light propagation, because $\Phi \equiv 0$ throughout, the photon-sphere condition for a static, spherically symmetric spacetime, $\Phi'(r) = 1/r$, is never satisfied ($\Phi' = 0$ for all $r > 0$). Thus, the zero-tidal-force wormhole has *no photon sphere* for any ζ_c. Light bending is nevertheless present and computable: for a photon with impact parameter B, the standard substitution $r = B/\cos\theta$ removes the turning-point singularity in the null-geodesic integral and yields the deflection angle in closed integral form,

$$\delta(B) = 2\int_0^{\pi/2} \frac{d\theta}{\sqrt{1-b_{\rm eff}(B/\cos\theta)/(B/\cos\theta)}} - \pi. \qquad (27)$$

Figure 13(b) shows $\delta(B)$ in the GR limit and for four Finslerian parameter values. At a fixed impact parameter, the deflection increases with ζ_c, consistent with the effectively larger throat geometry described by $b_{\rm eff}$.

D. Generalization: nonzero redshift function

Throughout this paper, we set $\Phi(r) \equiv 0$ to isolate the effect of the FR anisotropy field from conventional gravitational redshift. Relaxing this assumption is straightforward in principle: substituting a weak, decaying Newtonian-like potential $\Phi(r) = -\Phi_0 r_0/r$ into the general field equations, Eqs. (3)–(5), and expanding to linear order in Φ_0 yields closed-form corrections to Eqs. (13)–(15). We verified that these corrections reduce identically to our $\Phi = 0$ results when $\Phi_0 = 0$.

The main structural change is that the gravitational

CPC Accepted

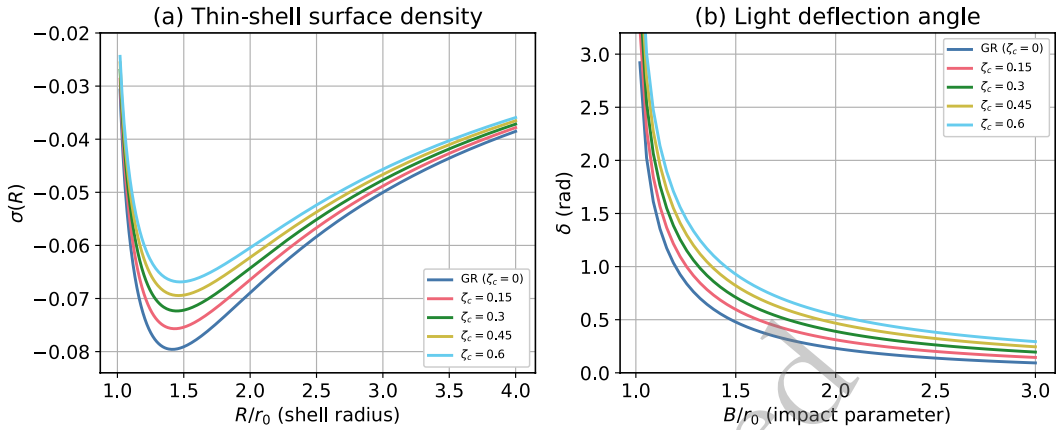


Fig. 13. (color online) (a) Thin-shell surface density given by Eq. (26). (b) Light-deflection angle given by Eq. (27) as a function of the impact parameter B.

force $F_g = -\frac{1}{2}\Phi'(\rho + p_r)$ in the generalized equilibrium equation, Eq. (22), is no longer identically zero. Consequently, the full force balance becomes $F_h + F_g + F_a + F_\zeta = 0$, with all four terms generally nonzero. A systematic reanalysis of the energy conditions, sound speeds, and stability diagnostics for $\Phi_0 \neq 0$–analogous to the complete treatment given here for $\Phi = 0$–is a natural extension of this work but is beyond the scope of the present paper. We record the linearized field equations and the reappearance of F_g here to facilitate that extension.

E. Comparison with other modified-gravity wormhole constructions

It is useful to place our results in the context of other geometric approaches to reducing the exotic-matter content of wormholes, several of which were cited in the Introduction. In $f(R)$ gravity, Harko et al. showed that specific choices of $f(R)$ can support a fixed Morris–Thorne-type geometry with matter satisfying the null and weak energy conditions everywhere. This constitutes a genuine elimination of exotic matter, albeit at the cost of a highly constrained, non-elementary form of $f(R)$ [35]. Constructions in $f(R,T)$ gravity typically yield an outcome closer to ours: NEC violation is confined to a finite region around the throat rather than eliminated outright, with the size of that region determined by the theory's coupling parameter [36–39]. The $f(Q)$ construction of Rastgoo and Parsaei similarly satisfies the energy conditions only over a bounded parameter range, rather than unconditionally [42]. Our FR result is closest to this second class of outcomes: as in the $f(R,T)$ and $f(Q)$ constructions, the geometric modification confines, rather than eliminates, the exotic region. This confinement is controlled by a single anisotropy parameter, ζ_c, which plays a role broadly analogous to the coupling constants in those theories; the size of the confined region is set by the same competition between throat-adjacent strength and large-r decay that we quantify in Sec. VI B. A distinctive feature of the present FR construction is that the same anisotropy field was shown, in an entirely separate calculation, to increase the maximum supported mass of compact stars [12]. To our knowledge, no comparably direct link between a compact-star observable and a wormhole observable, governed by the same single parameter, has been established for the $f(R,T)$, $f(Q)$, or Rastall-gravity constructions cited above [40, 41]. A fully quantitative side-by-side comparison, for instance, of $I_V^{\rm shell}$ across theories at a matched throat radius and a matched fractional deviation from GR would require a common convention for this measure across formalisms with substantially different field content. We leave this comparison as a natural extension of the present analysis.

VII. DISCUSSION AND CONCLUSION

We have constructed a traversable wormhole in Finsler–Randers gravity by specializing the general osculating-Riemannian field equations of Ref. [12] to a zero-tidal-force Morris–Thorne metric with shape function $b(r) = r_0^2/r$ and closing the system with a simple, decaying, weak-field ansatz for the FR anisotropy field, $\zeta_0(r) = \zeta_c r_0/r$. The resulting matter functions, Eqs. (13)–(15), reduce identically to the general-relativistic Morris–Thorne solution as $\zeta_c \to 0$.

Within the weak-anisotropy regime $\zeta_c \ll 1$ under which the field equations were derived (and, more precisely, within $\zeta_c \lesssim 0.3$, the practical range identified in Sec. III over which our quantitative results are reliable), we find that increasing ζ_c: (i) reduces the magnitude of the negative energy density near the throat, (ii) shrinks the radial extent of the NEC-violating region from the entire spacetime to a finite shell $r_0 \le r \le r_*(\zeta_c)$, and (iii) monotonically decreases the exotic-matter content confined to that shell. Formally, the NEC-violating shell vanishes at $\zeta_c = 2$; however, this value lies outside the strict validity range $|\zeta_0| \ll 1$ of the weak-field, osculating ap-

CPC Accepted

proximation used to derive Eqs. (3)–(5). We therefore do not claim a fully non-exotic wormhole solution here. Rather, the monotonic trend for $\zeta_c \lesssim 0.5$ demonstrates that Finslerian anisotropy can substantially reduce, without eliminating, the exotic-matter requirement of a fixed wormhole geometry, consistent with the way the same FR anisotropy was shown to increase the maximum supported mass of compact stars in Ref. [12].

We also derived the generalized hydrostatic-equilibrium equation for this class of solutions and showed that it acquires an explicit geometric force $F_\zeta(r)$, sourced by the radial gradient of $\zeta_0(r)$, in addition to the usual hydrostatic and pressure-anisotropy forces. As discussed in Sec. V, we interpret this term as an effective geometric exchange between the metric and anisotropy sectors of the theory rather than as an independent material force. This term vanishes identically in the GR limit and provides a clear diagnostic of the direct mechanical role of the Finslerian geometry in supporting the wormhole.

The extended analysis of Sec. VI, together with Secs. IV D–IV E, yields several further results. The radial tidal force vanishes identically for every observer and every ζ_c—an exact consequence of $\Phi \equiv 0$—whereas the lateral tidal force is nonzero, computable in closed form, Eq. (20), and grows modestly with ζ_c. Thus, the reduction in exotic matter comes at the cost of a slightly less gentle passage for a rapidly moving traveler. The equation-of-state and sound-speed diagnostics reveal a genuine limitation of the benchmark shape function $b = r_0^2/r$ itself, already present in its GR limit, where $v_t^2 = -1$ identically. We explicitly report this limitation: the FR correction does not cure the pathology and, in fact, shrinks the domain over which the diagnostic remains well-defined. Therefore, the associated Herrera cracking combination, as noted in Sec. IV E, should be interpreted only as a local indicator within that restricted domain and not as a global stability statement for the wormhole. We also corrected an initial overstatement: the fixed-shell exotic-matter quantifier used in Sec. IV diverges logarithmically as the shell size grows, and the properly convergent measure integrates only over the NEC-violating region itself. We adopt this convergent shell measure, $I_V^{\rm shell}(\zeta_c)$, as our primary quantitative measure of the amount of exotic matter required by the model; the fixed-shell value I_V of Sec. IV is retained only for continuity with the convention of Ref. [2] and should not be interpreted as a competing measure. The (n,k) parameter sweep of Sec. VI B shows that the critical anisotropy strength is, notably, independent of the shape-function power whenever the anisotropy field decays no faster than $1/r$ ($\zeta_c^{\rm crit} = 2/k$ for $k \le 1$), whereas decay at least as fast as $1/r^{n+1}$ ($k \ge n+1$) admits no finite critical value. Finally, we exhibited a thin-shell realization of the same geometry with a reduced surface exotic density, established the absence of a photon sphere as an exact consequence of $\Phi \equiv 0$, computed the light-deflection angle in closed integral form, linearized the field equations for a nonzero redshift function $\Phi(r) = -\Phi_0 r_0/r$ to show how the equilibrium equation regains a genuine gravitational force term F_g once the zero-tidal-force restriction is lifted, and compared, in Sec. VI E, the character of this reduction with wormhole constructions in $f(R)$, $f(R,T)$, and $f(Q)$ gravity. The FR reduction found here is comparable to the shell-confinement outcomes reported in $f(R,T)$ and $f(Q)$ gravity, whereas the full elimination of exotic matter, as found in specific $f(R)$ models, remains outside the weak-anisotropy regime considered here.

Natural extensions of this work include a comprehensive reanalysis of the energy conditions, sound speeds, and stability diagnostics for the nonzero-Φ_0 case introduced in Sec. VI, analogous to the complete treatment given here for $\Phi = 0$; extension of the analysis beyond linear order in ζ_0, for which the Cartan torsion contributions C_{abc} neglected here become relevant and could, in principle, permit genuinely non-exotic configurations even at $O(\zeta_0) \sim 1$; a fully self-consistent reparameterization of the areal radius using the angular sector $f_{\theta\theta} = r^2(1+\zeta_0)$, rather than the radial-sector diagnostic $b_{\rm eff}$ used here; and an examination of the stability of these solutions under linear radial perturbations, following the methodology used for FR compact stars in Ref. [12].

DATA AVAILABILITY STATEMENT

No datasets were generated or analyzed in the current study. This work is purely theoretical and does not involve observational or experimental data. Supporting calculations and graphical results can be made available from the corresponding author upon reasonable request.

DECLARATIONS: CONFLICT OF INTEREST

The authors declare that they have no known competing financial interests or personal relationships that could have appeared to influence the work reported in this paper.

STATEMENT OF FUNDING

This research received no external funding.

CPC Accepted

References

[1] M. S. Morris and K. S. Thorne, Am. J. Phys. **56**, 395 (1988)

[2] M. Visser, *Lorentzian Wormholes: From Einstein to Hawking* (AIP Press, New York, 1995).

[3] G. Randers, Phys. Rev. **59**, 195 (1941)

[4] D. Bao, S.-S. Chern, and Z. Shen, *An Introduction to Riemann–Finsler Geometry* (Springer, New York, 2000).
[5] P. Stavrinos, Gen. Relativ. Gravit. **44**, 3029 (2012)
[6] S. Basilakos, A. P. Kouretsis, E. N. Saridakis, and P. Stavrinos, Phys. Rev. D **88**, 123510 (2013)
[7] F. Rahaman, N. Paul, S. De, S. Ray, and M. A. K. Jafry, Eur. Phys. J. C **75**, 564 (2015)
[8] J. Praveen, S. Narasimhamurthy, and B. Yashwanth, Eur. Phys. J. C **84**, 597 (2024)
[9] F. Rahaman, N. Paul, A. Banerjee, S. De, S. Ray, and A. Usmani, Eur. Phys. J. C **76**, 246 (2016)
[10] K. N. Singh, F. Rahaman, D. Deb, and S. Maurya, Front. Phys. **10**, 1038905 (2023)
[11] K. P. Das and U. Debnath, Eur. Phys. J. C **83**, 821 (2023)
[12] J. Praveen, R. Kumar, and S. K. Narasimhamurthy, Eur. Phys. J. C **86**, 806 (2026)
[13] L. Herrera, Phys. Lett. A **165**, 206 (1992)
[14] L. Herrera, Phys. Rev. D **97**, 044010 (2018)
[15] A. Einstein and N. Rosen, Phys. Rev. **48**, 73 (1935)
[16] J. A. Wheeler, Phys. Rev. **97**, 511 (1955)
[17] M. S. Morris, K. S. Thorne, and U. Yurtsever, Phys. Rev. Lett. **61**, 1446 (1988)
[18] M. Visser, Phys. Rev. D **39**, 3182 (1989)
[19] V. P. Frolov and I. D. Novikov, Phys. Rev. D **42**, 1057 (1990)
[20] D. Hochberg and M. Visser, Phys. Rev. D **56**, 4745 (1997)
[21] D. Hochberg and M. Visser, Phys. Rev. Lett. **81**, 746 (1998)
[22] D. Hochberg and M. Visser, Phys. Rev. D **58**, 044021 (1998)
[23] T. P. Sotiriou and V. Faraoni, Rev. Mod. Phys. **82**, 451 (2010)
[24] S. Nojiri and S. D. Odintsov, Phys. Rept. **505**, 59 (2011)
[25] S. Capozziello and M. De Laurentis, Phys. Rept. **509**, 167 (2011)
[26] T. Clifton, P. G. Ferreira, A. Padilla, and C. Skordis, Phys. Rept. **513**, 1 (2012)
[27] T. Harko, F. S. N. Lobo, S. Nojiri, and S. D. Odintsov, Phys. Rev. D **84**, 024020 (2011)
[28] T. Harko, Phys. Lett. B **669**, 376 (2008)
[29] T. Harko and F. S. N. Lobo, Eur. Phys. J. C **70**, 373 (2010)
[30] J. Beltrán Jiménez, L. Heisenberg, and T. Koivisto, Phys. Rev. D **98**, 044048 (2018)
[31] Y. Xu, G. Li, T. Harko, and S.-D. Liang, Eur. Phys. J. C **79**, 708 (2019)
[32] R. Ferraro and F. Fiorini, Phys. Rev. D **75**, 084031 (2007)
[33] G. R. Bengochea and R. Ferraro, Phys. Rev. D **79**, 124019 (2009)
[34] F. S. N. Lobo and M. A. Oliveira, Phys. Rev. D **80**, 104012 (2009)
[35] T. Harko, F. S. N. Lobo, M. K. Mak, and S. V. Sushkov, Phys. Rev. D **87**, 067504 (2013)
[36] M. Zubair, S. Waheed, and Y. Ahmad, Eur. Phys. J. C **76**, 444 (2016)
[37] M. Zubair, Q. Muneer, and S. Waheed, Eur. Phys. J. Plus **137**, 755 (2022)
[38] A. Chanda, S. Dey, and B. C. Paul, Gen. Relativ. Gravit. **53**, 78 (2021)
[39] A. Banerjee, M. K. Jasim, and S. G. Ghosh, Ann. Phys. **433**, 168575 (2021)
[40] S. Halder, S. Bhattacharya, and S. Chakraborty, Mod. Phys. Lett. A **34**, 1950095 (2019)
[41] Y. Heydarzade and M. Ranjbar, Eur. Phys. J. Plus **138**, 703 (2023)
[42] S. Rastgoo and F. Parsaei, Eur. Phys. J. C **84**, 623 (2024)
[43] G. S. Asanov, *Finsler Geometry, Relativity and Gauge Theories* (Springer, Dordrecht, 2012).
[44] H. Rund, *The Differential Geometry of Finsler Spaces* (Springer, Berlin, 2012).
[45] P. Stavrinos, A. Kouretsis, and M. Stathakopoulos, Gen. Relativ. Gravit. **40**, 1403 (2008)
[46] A. Kouretsis, M. Stathakopoulos, and P. Stavrinos, Phys. Rev. D **79**, 104011 (2009)
[47] A. Kouretsis, M. Stathakopoulos, and P. Stavrinos, Phys. Rev. D **82**, 064035 (2010)
[48] A. Kouretsis, M. Stathakopoulos, and P. Stavrinos, Math. Methods Appl. Sci. **37**, 223 (2014)
[49] S. Basilakos and P. Stavrinos, Phys. Rev. D **87**, 043506 (2013)
[50] P. C. Stavrinos and M. Alexiou, Int. J. Geom. Methods Mod. Phys. **15**, 1850039 (2018)
[51] G. Papagiannopoulos, S. Basilakos, A. Paliathanasis, S. Pan, and P. Stavrinos, Eur. Phys. J. C **80**, 816 (2020)
[52] E. Kapsabelis, E. N. Saridakis, and P. Stavrinos, Eur. Phys. J. C **84**, 538 (2024)
[53] A. Triantafyllopoulos, S. Basilakos, E. Kapsabelis, and P. Stavrinos, Eur. Phys. J. C **80**, 1200 (2020)
[54] R. Hama, T. Harko, S. V. Sabau, and S. Shahidi, Eur. Phys. J. C **81**, 742 (2021)
[55] S. I. Vacaru, Class. Quantum Gravity **27**, 105003 (2010)
[56] Z. Nekouee, S. Narasimhamurthy, and S. Pacif, J. Cosmol. Astropart. Phys. **04**, 061 (2024)
[57] A. Ditta, R. Manzoor, F. Javed, M. Aslam, M. Y. Malik, and G. Belalova, Phys. Dark Universe **48**, 101873 (2025)

CPC Accepted